Kinetics of quenched systems with long-range repulsive interactions

Christopher Roland and Rashmi C. Desai
Department of Physics, University of Toronto, Toronto, Ontario, Canada M5S 1A7
(Received 20 February 1990; revised manuscript received 11 April 1990)

The kinetics of a quenched system with a nonconserved order parameter having both an attractive and a long-range repulsive interaction (specifically a uniaxial ferromagnetic film) is studied. The presence of the repulsive interaction leads to the formation of periodically modulated structures. For various physical situations, the kinetics is studied through numerical integration of the appropriate Langevin equation. As the strength of the repulsive interaction is increased, we find that at intermediate times the effective domain-growth exponent decreases continuously from one-half to zero. For the case of a system in zero external field and at zero temperature, we have constructed a dynamical theory based on a singular perturbation expansion. The theory compares well with the results of numerical simulation. It accounts for the formation of modulated domain structures with sharp interfaces and the saturation of the order parameter but not the late-stage phenomena.

I. INTRODUCTION

When a system in a high-temperature homogeneous state is rapidly quenched to a temperature well below its ordering temperature it orders kinetically. A long-wavelength instability amplifies the fluctuations in the initial state leading to the formation of domains of macroscopic size.[1] At late time, phase-separating systems are usually characterized by a single time-dependent length, the average domain size $R(t)$, which grows as a power law $R \sim t^n$. The growth exponent is a characteristic of the mechanism driving the phase separation. Through it, phase separating systems may be classified into a small number of universality classes, where each member of a given class shares the same kinetic properties. These universality classes depend crucially upon the presence or absence of conservation laws. For a system with a scalar nonconserved order parameter (Model A), the growth is curvature driven with $n=\frac{1}{2}$,[2] while a long-range diffusion mechanism gives $n=\frac{1}{3}$ for systems with a conserved order parameter (Model B).[3]

This scenario assumes attractive interactions between constituents. However, there are many systems which are characterized by both short-range attractive interactions and relatively weaker long-range repulsive interactions. In equilibrium, system with both attractive and repulsive interactions exhibit a rich variety of spatially modulated phases termed supercrystals. Examples of such systems include uniaxial ferromagnetic films,[4] lipid monolayers,[5] ferrofluid systems,[6] cholesteric liquid crystals,[7] charge-density-waves,[8] and the primate visual cortex.[9]

In this paper, we study the dynamics of quenched systems with a scalar nonconserved order parameter and a long-range repulsive interaction. As a specific example, we treat the time evolution of quenched uniaxial ferromagnetic films. Here there is a competition between the short-range attractive forces which favor alignment and the long-range repulsive interactions which favor anti-alignment. This leads to the formation of modulated phases with either lamellar or hexagonal symmetry.

Introducing a long-range repulsive force changes the intrinsic nature of the model from a local to a nonlocal model. A novel feature is that by changing the parameters which characterize the repulsive force, one can tune the form of the linear growth exponent in such a way, as to move continuously from a system where the long-wavelength modes are unstable to a system where the long-wavelength modes are stable. The effect of increasing the repulsive force strength is such that (i), the maximally unstable wave number moves from a zero to a nonzero value, and (ii) the linear growth exponent for zero wave number decreases from a positive value through zero to negative values where, unlike Model-A or Model-B systems, the long-wavelength modes become stable, so that it is a band of unstable modes which amplifies the fluctuations in the initial state.

We find that the time evolution of these modulated phases occur in two stages: an early-time and a late-time regime. In the early-time regime, the instability amplifies the fluctuations present in the initial conditions, saturates them, and forms sharp interfaces. This time regime is dominated by $k_{\max}$ the maximally unstable wave number of the linear dispersion relation. In contrast, the late-time regime is dominated by $k_{\rm eq}$, the wave number of the equilibrium modulated structure. The late-time dynamics is therefore characterized by crossover phenomena, as the characteristic wave number of the system changes from $k_{\max}$ to $k_{\rm eq}$. However, in some cases, $k_{\rm eq}$ and $k_{\max}$ are not too different, so that this shift may be difficult to observe. Because the late-time evolution of the system is ultimately governed by a single time-independent length scale, the system does not display self-similarity. Furthermore, the free energy of many modulated system is degenerate with respect to the direction of $\mathbf{k}_{\rm eq}$, i.e., the free energy is a function of $k_{\rm eq}$, not $\mathbf{k}_{\rm eq}$. A quench from a

high-temperature state to a state well below its ordering temperature therefore results in the formation of a pattern of modulated phase broken up by dislocations. The presence of these unbound dislocations and the free-energy barriers associated with these dislocations effectively pins the interfaces at low temperatures and prevents the system from forming modulated structures on long-length scales. In this paper, we will concentrate on the early-time regime, leaving a quantitative discussion of the late stages for the future.

During the early-time regime, the unstable modes are responsible for the increase of the order parameter. For critical quenches we find in the early-time regime that a convoluted and interconnected domain structure with sharp phase boundaries is formed. We study the dynamics of this regime by concentrating on a model modified for a system with a long-range repulsive force. This leads to a nonlinear time-dependent Ginzburg-Landau (TDGL) equation. (In the absence of the repulsive force the model reduces to Model A. In zero external field and zero temperature the TDGL equation may be solved through iterations. The resultant singular perturbation expansion may be approximately summed in a manner similar to that of Kawasaki, Yalabik, and Gunton (KYG).[10] The approximate solution obtained in this manner predicts a nonexponential growth of the order parameter and its saturation at values well within ± 1, the saturation value for Model A systems. The growth rates and saturation values compare favorably with those obtained from the numerical integration of the TDGL equation.

The TDGL equations are given in Sec. II of this paper. These equations are considered for the specific case of a uniaxial ferromagnetic film, whose equilibrium phases are also briefly reviewed. In Sec. III, the early-time dynamics of the system quenched into the "stripe" phase is discussed. Both the linear solution and a solution based on the KYG expansion are considered. In Sec. IV numerical results are presented for quenches (to zero temperature) both into the stripe and hexagonal region of the phase diagram. In particular, we have studied the domain growth, the structure factor, and the one-point distribution function of the order parameter. A comparison between the early-time models and the numerical results at zero temperature are also given. A summary of our conclusions is given in Sec. V.

II. MODEL

The model we consider is based on nonlinear TDGL equations for a system with a scalar, nonconserved order parameter with the free energy modified in such a way as to account for the contribution of the long-range repulsive force. The time derivative of the order-parameter fluctuations (ϕ) is then related to the coarse-grained free-energy functional in the following way:

$$\frac{\partial\phi(\mathbf{r},t)}{\partial t}=-M\frac{\delta F}{\delta\phi}+\zeta(\mathbf{r},t)\ , \tag{1}$$

where M is the mobility which is assumed to be a constant and $\zeta(\mathbf{r},t)$ the Gaussian random noise which derives from the coarse-graining procedure. It is related to M through a fluctuation-dissipation relation:

$$\langle\zeta(\mathbf{r},t)\zeta(\mathbf{r}',t')\rangle=2k_BTM\delta(\mathbf{r}-\mathbf{r}')\delta(t-t')\ , \tag{2}$$

where k_B is the Boltzmann constant and T the temperature of the system. The free-energy functional now consists of both a local and a nonlocal term:

$$F\{\phi\}=F_L\{\phi\}+F_{\rm NL}\{\phi\}\ , \tag{3}$$

where

$$F_L\{\phi\}=\int d^dr\left[f(\phi)+\frac{\kappa}{2}(\nabla\phi)^2\right]\ , \tag{4}$$

$$F_{\rm NL}\{\phi\}=\frac{\alpha}{2}\int d^dr\,d^dr'\phi(\mathbf{r}')g(|\mathbf{r}-\mathbf{r}'|)\phi(\mathbf{r}')\ , \tag{5}$$

where κ and α are positive phenomenological constants related to the range of the short-range attractive force and the strength of the long-range repulsive interaction $g(|\mathbf{r}-\mathbf{r}'|)$, respectively. The bulk free energy is assumed to have a stable single-well structure if the temperature is greater than the ordering temperature T_c, i.e.,

$$f(\phi)=\frac{r_{\rm eq}}{2}\phi^2\ , \tag{6}$$

and a double-well structure if $T<T_c$:

$$f(\phi)=\frac{-r_{\rm ne}}{2}\phi^2+\frac{u}{4}\phi^4+H\phi\ . \tag{7}$$

Here $r_{\rm eq}$, $r_{\rm ne}$, and u are also positive phenomenological constants and H the magnitude of an external field which couples linearly to the order parameter. Without $F_{\rm NL}$ (i.e., $\alpha=0$), the aforementioned equations simply describe the dynamics of a system with a nonconserved, scalar order parameter, i.e., Model A. All of the new physics pertaining to the long-range repulsive forces arises from the extra term $F_{\rm NL}$.

The set of transformations

$$\begin{aligned}\mathbf{x}&=\left[\frac{r_{\rm ne}}{\kappa}\right]^{1/2}\mathbf{r}\ ,\\ \psi&=\left[\frac{u}{r_{\rm ne}}\right]^{1/2}\phi\ ,\\ \tau&=(Mr_{\rm ne})t\ ,\end{aligned} \tag{8}$$

brings the equations of motion for the two-phase region into a dimensionless form:

$$\begin{aligned}\frac{\partial\psi(\mathbf{x},\tau)}{\partial\tau}&=\nabla^2\psi(\mathbf{x},\tau)+\psi(\mathbf{x},\tau)-\psi^3(\mathbf{x},\tau)-h\\ &\quad+\sqrt{\epsilon}\mu(\mathbf{x},\tau)-\beta\int d^dx'\psi(\mathbf{x}',\tau)g(|\mathbf{x}-\mathbf{x}'|)\ ,\end{aligned} \tag{9}$$

where

$$\langle\mu(\mathbf{x},\tau)\mu(\mathbf{x}',\tau')\rangle=\delta(\mathbf{x}-\mathbf{x}')\delta(\tau-\tau')$$

and

$$\beta=\frac{\alpha}{r_{\rm ne}}\left[\frac{\kappa}{r_{\rm ne}}\right]^{d/2},$$
$$h=\left[\frac{u}{r_{\rm ne}}\right]^{1/2}\frac{H}{r_{\rm ne}}, \tag{10}$$
$$\epsilon=\frac{2k_BT_f\mu}{r_{\rm ne}^2}\left[\frac{r_{\rm ne}}{\kappa}\right]^{d/2}$$

are the three main dimensionless parameters describing the model. They represent the strength of the long-range force, the external field, and the strength of the thermal noise, respectively. [Note that the function $g(|\mathbf{x}-\mathbf{x}'|)$ may contain further parameters.] Introducing the Fourier transform

$$\psi_{\mathbf{k}}(\tau)=\int d^dx e^{i\mathbf{k}\cdot\mathbf{x}}\psi(\mathbf{x},\tau), \tag{11}$$

converts (9) into

$$\frac{\partial\psi_{\mathbf{k}}(\tau)}{\partial\tau}=\gamma_k\psi_{\mathbf{k}}(\tau)-\sum_{k'}\sum_{k''}\psi_{\mathbf{k}'}\psi_{\mathbf{k}''}\psi_{\mathbf{k}-\mathbf{k}'-\mathbf{k}''}(\tau)$$
$$-h\delta(k)+\sqrt{\epsilon}\mu_k, \tag{12}$$

with a linear dispersion relation

$$\gamma_{\mathbf{k}}=1-k^2-\beta g(k). \tag{13}$$

Here $g(k)$ is the Fourier transform of $g(x)$.

The equation of motion for the single-phase region of the phase diagram is readily found using (1)–(6). The corresponding stationary solution for the structure factor $\langle|\psi|^2(k,\infty)\rangle$ has the modified Orstein-Zernike form

$$\langle|\psi|^2(k,\infty)\rangle=\frac{\epsilon_I}{1+k^2+\beta g(k)}. \tag{14}$$

where $\epsilon_I=\epsilon(r_{\rm ne}T_f/r_{\rm eq}T_i)$ in two dimensions. Here T_i and T_f represent the initial and final quench temperatures, respectively. This is the structure factor for the prequench state, and defines $\langle|\psi|^2(k,\tau=0)\rangle$ for the quenched state.

As an example of the aforementioned, we consider a uniaxial ferromagnetic film whose equilibrium properties we now briefly review. Such systems have in the past received considerable attention in connection with bubble memory applications[11] and more recently in the context of topological melting.[12] The system consists of a finite film of a strongly uniaxial magnetic material. The thickness of the film in the $\hat{\mathbf{z}}$ direction is denoted by L. In the xy plane the film is assumed to be very large and isotropic (in the disordered phase). Assuming straight domain walls in the $\hat{\mathbf{z}}$ direction allows us to treat the film as a two-dimensional system. The order parameter is taken to be the magnetization averaged over the $\hat{\mathbf{z}}$ direction. The external magnetic field is oriented along the $\hat{\mathbf{z}}$ direction.

This system is characterized by a balance between the cost of forming a domain wall and its magnetostatic self-energy. The latter gives a contribution

$$F_D=\tfrac{1}{2}\int dS\sigma\Phi \tag{15}$$

to the free energy. Here, the integral is taken over the surface of the formed domains, σ is the magnetic charge distribution on the surfaces created by the nonzero magnetization, and Φ is the magnetic potential. The uniaxial ferromagnetic film can reduce this magnetostatic energy easily by forming domains of ordered phases with alternating sign. The system which contains N domains has a free energy which is about $1/N$ times lower than that of a uniformly magnetized film. Hence, the formation of modulated structures is favored. The free energy of the system can readily be written in the form of Eq. (3), with a long-range repulsive force given by

$$g(|\mathbf{x}-\mathbf{x}'|)=\frac{1}{|\mathbf{x}-\mathbf{x}'|}-\frac{1}{[(\mathbf{x}-\mathbf{x}')^2+L^2]^{1/2}}$$
$$=\int d\mathbf{k}\frac{(1-e^{-Lk})}{k}e^{i\mathbf{k}\cdot(\mathbf{x}-\mathbf{x}')}, \tag{16}$$

with a strength $\alpha\sim(g\mu_B)^2$, where $g\mu_B$ is the appropriate gyromagnetic coefficient of the material.[13] For $|\mathbf{x}-\mathbf{x}'|$ large compared to L, $g(|\mathbf{x}-\mathbf{x}'|)$ approaches $L^2/(2|\mathbf{x}-\mathbf{x}'|^3)$ which is like a repulsive dipolar force.

The equilibrium states of this system are obtained by studying the solutions of $\delta F/\delta\phi=0$, as discussed in detail by Garel and Donaich.[4] The phase diagram is illustrated in Fig. 1. The system spontaneously forms two types of supercrystal phases when quenched well below its ordering temperature: a lamellar or "stripe" phase and "bubble" or hexagonal phase. The stripe phase is formed in zero or small external field. Near the critical temperature, in one dimension, the equilibrium solution is well approximated by a single-mode expansion $\psi(x)\sim\cos(k_{\rm eq}^{(u)}x)$. The amplitude and spatial period $k_{\rm eq}^{(u)}$ may both be found by minimizing the free energy. It is straightforward to show that within the single-mode approximation, $k_{\rm eq}^{(u)}$ is given by

$$\frac{d\gamma(k)}{dk}=0, \tag{17}$$

i.e., $k_{\rm eq}^{(u)}$ is the same as $k_{\rm max}$ the maximally unstable mode of the linear dispersion relation. At low temperatures, this single-mode approximation is no longer valid and $k_{\rm eq}$

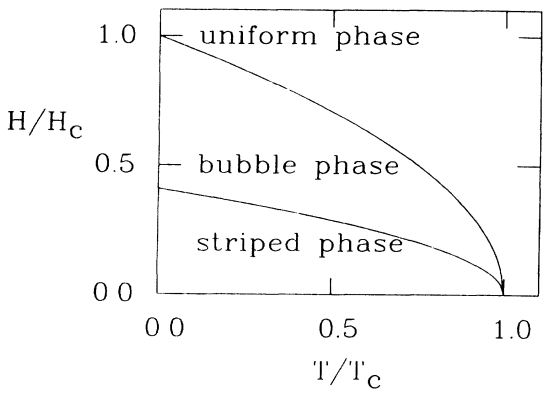

FIG. 1. A sketch of the phase diagram for uniaxial ferromagnetic film, in normalized units. Here T_c is the critical temperature and H_c the critical field value marking the transition between the uniform and bubble phase.

will differ from k_{max}. This approximation overestimates the wall energy, so that k_{max} provides an upper bound to k_{eq}. A lower bound to k_{eq} is found by approximating the modulated stripe structure is a series of domains with hard domain walls. Then, $k_{eq}^{(l)}$ is the solution of[4]

$$\frac{d}{dk}\left[k+\beta\sum_{n=0}^{\infty}\frac{1}{(2n+1)^3}\frac{(1-e^{-(2n+1)Lk})}{k}\right]=0\ . \qquad (18)$$

The two approximations are shown in Fig. 2. Note that $k_{eq}^{(l)}$ is always less than k_{max}. In the limit of large L (at constant β), the stripe width is relatively narrow so that the amount of wall energy is considerable. Here, $\psi(x)$ is well approximated by the single-mode expansion so that k_{eq} is close to k_{max}. On the other hand, if L is small, the stripe width is very large so that domain walls appear as hard walls, and then $k_{eq}^{(l)}$ provides a better approximation to k_{eq}. Thus, we expect that the exact k_{eq} will, while remaining within the two bounds shown in Fig. 2, move from the lower bound for small L, to the upper bound for large L.

In two dimensions the equilibrium solution is still a stripe solution. However, a quench from an initially disordered state results in configurations broken up by dislocations because of the degeneracy of the free energy with respect to the orientations of vector $\mathbf{k}_{eq}$. As a result, the morphology created has a labyrinthian appearance. It has been shown, that these dislocations are always unbounded.[4] As a result the system displays short-range but no long-range order.

The hexagonal phase, which exists only in relatively high nonzero fields, is similarly characterized. A quench from a two-dimensional disordered system results in the formation of configurations broken up by dislocations. In contrast to the stripe phase, however, there is a finite-temperature Kosterlitz-Thouless transition temperature, below which the dislocations will be bound. The transition between the two modulated phases is a first-order transition and will not be discussed in this paper.

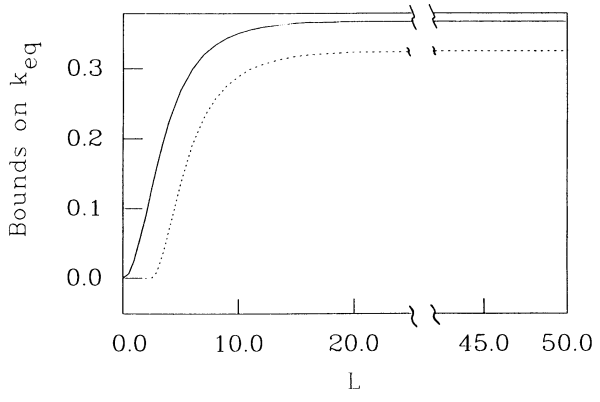

FIG. 2. The variation of k_{eq} as predicted by the single-mode approximation (solid line) and from a model with hard domain walls (dashed line). The solid line gives an upper bound and the dashed line gives a lower bound to k_{eq}.

III. EARLY-TIME THEORY

In this section we consider the dynamics of a system which has been quenched from an initially disordered paramagnetic state into the stripe phase. We first present the linear solution, which is valid for very early times only. Here, the presence of the long-range force changes the nature of the initial instability: depending on the parameters (β,L) of the repulsive force, the long-wavelength fluctuations in the order parameter may or may not be unstable. The maximally unstable wave number occurs at a nonzero k value, as long as $\beta\neq 0$.

An approximate solution to (12) with $\beta=0$ was given by Kawasaki, Yalabik, and Gunton (KYG).[10] The KYG solution, which is based on a singular perturbation expansion accounts for some of the nonlinearities present in the TDGL formulation. Specifically, it correctly predicts the saturation of the order parameter and the formation of sharp interfaces. It does not account for the coarsening effects. In the latter part of this section, we describe the KYG-like solution for (12) with $\beta\neq 0$. A comparison between this solution and a numerical integration of the TDGL equations is given in Sec. IV.

Linearizing (12), and introducing the two-point correlation function,

$$\langle\psi(\mathbf{k},\tau)\psi(\mathbf{k}',\tau)\rangle=(2\pi)^d\delta(\mathbf{k}-\mathbf{k}')\langle|\psi|^2\rangle(\mathbf{k},\tau)\ , \qquad (19)$$

one readily obtains the linear structure theory,

$$\langle|\psi|^2\rangle(k,\tau)=\langle|\psi|^2\rangle(k,\tau=0)e^{2\gamma_k\tau}+\epsilon\left[\frac{e^{2\gamma_k\tau}-1}{2\gamma_k}\right]+h^2\left[\frac{1-e^{\gamma_k\tau}}{\gamma_k}\right]^2\ , \qquad (20)$$

where $\gamma_k=1-k^2-\beta(1-e^{-kL})/k$. Figure 3 illustrates the linear dispersion relation γ_k versus k in three

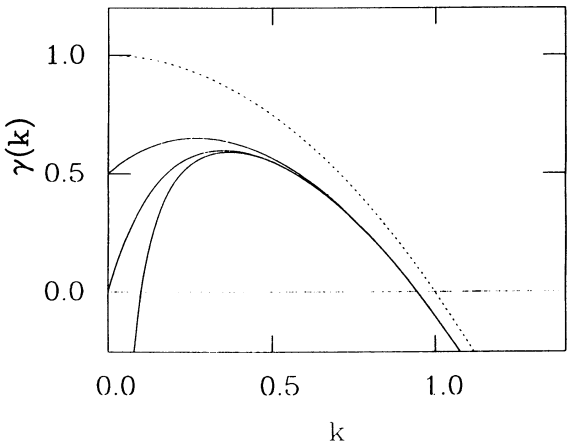

FIG. 3. Linear-dispersion relation γ_k vs k for a system with a nonconserved order parameter and long-range repulsive force. Positive k values are unstable. Three cases are possible: systems with unstable long-wavelength modes shown by the upper solid line (parameters $L=5$ and $\beta=0.1$); systems with the $k=0$ mode being marginally stable ($L=10$ and $\beta=0.1$); systems with stable long-wavelength modes shown by the lower solid line ($L=50$ and $\beta=0.1$). For comparison the dashed line shows the dispersion relation for a Model-A system.

different limits, and compares it to the more familiar case of a Model A phase-separating system. The effect of the long-range force is to move the maximally unstable k mode away from $k=0$ to a finite value $k_{\max}$. It is this maximally unstable mode which determines the period of the initial modulated formed.

For a uniaxial ferromagnetic system, with a repulsive interaction as given by (16), the instability is controlled by the strength of the long-range force (β) and the thickness of the film (L). The maximally unstable wave number $k_{\max}$ is given as the solution of the equation

$$2k_{\max}^3=\beta(1-(1+k_{\max}L)e^{-Lk_{\max}}) . \tag{21}$$

If $Lk \gg 1$, then $\gamma_k \approx 1-k^2-\beta/k$, which is independent of L. On the other hand, for small values of Lk, $\gamma_k \approx 1-\beta L+\beta L^2 k/2$. Clearly, if $L<1/\beta$, then the $k=0$ mode is unstable, so that the order parameter of the system is not conserved. On the other hand, if $L>1/\beta$, then the long-wavelength modes are stable and decay away, so that it is a narrow band of unstable modes which amplifies the fluctuations in the initial state. $L=1/\beta$ is a special value because there is a cancellation of the k-independent terms arising from the bulk free energy on one hand, and the long-range repulsive force on the other. This has the consequence that the leading small-k behavior of γ_k is linear in k. For such a system, the linear term is absent for the $k=0$ mode and the nonlinearities determine its evolution; however, because these nonlinearities are small at early times, the average order parameter $\psi_{k=0}(\tau)$ appears time invariant at early times in the simulations.

While the linear solution correctly identifies the unstable modes, it incorrectly predicts an unbounded, exponential growth of the order parameter for these wave numbers. Such a solution can only be valid for very early times. To obtain a nonzero growth rate, on the one hand, and the saturation of the order parameter on the other, the nonlinearities must be taken into account. Formally, Eq. (12), for zero field and at zero temperature can be written in an integral form

$$\psi_{\mathbf{k}}(\tau)=\psi_{\mathbf{k}}^0(\tau)-\int_0^\tau d\tau' e^{\gamma_k(\tau-\tau')}\sum_{k'}\sum_{k''}\psi_{\mathbf{k}'}\psi_{\mathbf{k}''}\psi_{\mathbf{k}-\mathbf{k}'-\mathbf{k}''}(\tau') , \tag{22}$$

where

$$\psi_{\mathbf{k}}^0(\tau)=\psi_{\mathbf{k}}(\tau=0)e^{\gamma_k\tau} \tag{23}$$

is the linear solution. This equation may now be solved iteratively using the linear solution. The result is an infinite singular perturbation expansion. The difficulty with this approach is that each term grows more exponentially in time than the one preceding it, so that all terms must be retained in order to obtain a physically meaningful solution. Kawasaki *et al.*[10] extending the work of Suzuki,[14] were able to obtain an approximate solution for a Model A system. Even though the structure of the equations for a system with long-range repulsive interaction and Model A are formally identical, they differ in the evaluation of the vertex, i.e., γ_k, whereas for Model A the maximum of γ_k occurs at $k=0$, for the problem defined by (12), (13), and (16), the maximum is shifted to a nonzero k as shown in Fig. 3.

The steps required to obtain an approximate solution are now sketched. Details are similar to those given in Ref. 10, so we will only highlight the differences.[15] The first step is to note that asymptotically the nth order term in the expansion can be written in terms of a diagram D_n, multiplied by the appropriate combinatorial factor; i.e.,

$$\psi_{\mathbf{k}}(\tau)=\sum_{n=0}^{\infty}(2n-1)!!D_n . \tag{24}$$

Graphically, this is illustrated in Fig. 4. Here, the thick line represents the solution ψ_k, while the thin line represents the linear solution ψ_k^0. The general nth order diagram is

$$D_n=(-1)^n e^{\gamma_k\tau}\sum_{\mathbf{k}_1}\sum_{\mathbf{k}_2}\cdots\sum_{\mathbf{k}_{2n+1}}\delta\left[\mathbf{k}-\sum_{i=1}^{2n+1}\mathbf{k}_i\right]\left[\prod_{i=1}^{2n+1}\psi_{k_i}(\tau=0)\right]f_n(\{s_n\};\tau) , \tag{25}$$

where

$$f_n(\{x\};\tau)=\int_0^\tau d\tau_1\int_0^{\tau_1}d\tau_2\cdots\int_0^{\tau_{n-1}}d\tau_n\exp\left[\sum_{i=1}^n x_i\tau_i\right] , \tag{26}$$

with

$$x_i=\gamma_{k_{2i-1}}+\gamma_{k_{2i}}+\gamma_{s_1}-\gamma_{s_2} , \tag{27}$$

where $S_1=\sum_{j=2i+1}^{2n+1}k_j$ and $S_2=\sum_{j=2,i-1}^{2n+1}k_j$. The time integrals may be evaluated in a straightforward way, by taking the Laplace transform of D_n, splitting the resultant term into partial fractions, and performing the integration for the dominant term only. This introduces an error of order $\sqrt{\tau/4\ln 4}e^{-2\gamma_{k_{\max}}\tau}$. Then, assuming that the dominant contribution to the integrals occurs when $k_i \approx k_{\max}$, one is able to evaluate D_n using the method of Laplace. This approximation is necessary here because the long-range interaction has shifted the maximally unstable mode away from the origin. This assumption implies that all of the k vectors arrange themselves in an isotropic fashion about $k_{\max}$. This is, to a large extent, an uncontrolled approximation. As a result, the KYG-type of solution to the model is incapable of describing any shift in the position of $k_{\max}$. This feature makes it difficult to apply the KYG approach to systems in which coarsening phenomena play a major role (e.g., Model B). KYG-type solutions seem, at present, to be restricted to

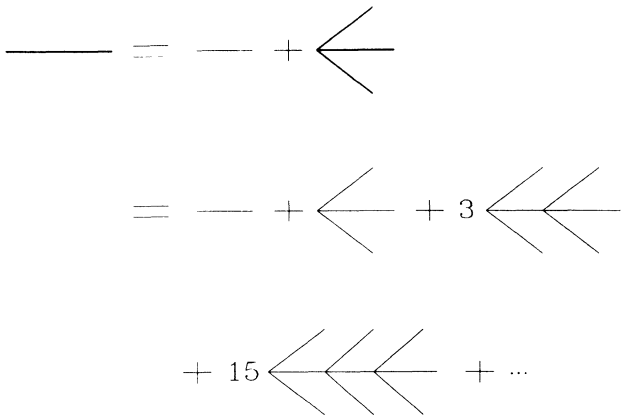

FIG. 4. Graphical representation of the KYG expansion, for which the nth order branched diagrams are given by the nth order pine tree diagram D_n. Here, a thick line indicates $\psi_k(\tau)$, while ψ_k^0 is indicated by a thin line.

systems having a single dominant and stationary wave vector.

For a uniaxial ferromagnetic film, the inability of the KYG solution to incorporate a shift in $k_{\max}$ restricts its validity as a description for the system's dynamics to the early-time regime. During the early-time regime, the dynamics of the system is dominated by $k_{\max}$. However, at equilibrium the system is characterized by stripes having wave number $k_{\rm eq}$. Therefore, at late times, a crossover must take place as the modulation length changes from $\lambda=2\pi/k_{\max}$ to $\lambda=2\pi/k_{\rm eq}$. Our KYG solution does not incorporate this shift, and so cannot account for this late-time crossover phenomena. In many cases, especially when $\beta L>1$, $k_{\max}$ is so close to $k_{\rm eq}$ that no late-time crossover is observed.

Straightforward but rather tedious algebra gives the nth-order diagram

$$D_n \approx \frac{\Gamma(\alpha_k)}{\Gamma(n+\alpha_k)}(-2\gamma_{k_{\max}})^{-n}\sum_{\mathbf{x}} e^{i\mathbf{k}\cdot\mathbf{x}}[\psi^0(\mathbf{x},\tau)]^{2n+1} , \tag{28}$$

with

$$\alpha_k=\frac{3\gamma_{k_{\max}}-\gamma_k}{2\gamma_{k_{\max}}} , \tag{29}$$

where $\psi^0(\mathbf{x},\tau)$ is the inverse Fourier transform of $\psi_k^0(\tau)$. Substitution of this result into (24) readily gives the result

$$\psi_k(\tau)=\sum_{\mathbf{x}} e^{i\mathbf{k}\cdot\mathbf{x}}\psi^0(\mathbf{x},\tau)F(\tfrac{1}{2},1;\alpha_k;z) , \tag{30}$$

with

$$z=\frac{-[\psi^0(\mathbf{x},\tau)]^2}{\gamma_{k_{\max}}} , \tag{31}$$

where F is the hypergeometric function.[16] This equation may be regarded as the central prediction of the KYG-type solution. Approximating $\alpha_k\approx 1$ (Ref. 17) gives a result similar to the one derived by Kawasaki *et al.*

$$\psi(\mathbf{x},\tau)=\frac{\psi^0(\mathbf{x},\tau)}{\{[1+\psi^0(\mathbf{x},\tau)]^2/\gamma_{k_{\max}}\}^{1/2}} . \tag{32}$$

This solution may be regarded as a time transformation $\psi(\tau=0)\rightarrow\psi(\tau)$. The probability distribution function may now be obtained in a straightforward way, by substitution of the nonlinear, inverse transformation of the order parameter

$$\psi^0(\mathbf{x},\tau)=\psi(\mathbf{x},\tau)/[1-\psi(\mathbf{x},\tau)^2/\gamma_{k_{\max}}]^{1/2} , \tag{33}$$

into the initial probability distribution function, which is assumed to be a Gaussian distribution centered about $\psi=0$.[10] The time-dependent probability function is, therefore, always a Gaussian in terms of the nonlinear variables defined above with a time-dependent variance. Note that the value of ψ has a predicted saturation value of $(\gamma_{k_{\max}})^{1/2}$. Finally, with the use of (32) the structure factor is readily obtained as[15]

$$\langle|\psi|^2\rangle(\mathbf{k},\tau)=\frac{\gamma_{k_{\max}}}{\pi}\sum_{\mathbf{x}_1,\mathbf{x}_2} e^{i\mathbf{k}\cdot(\mathbf{x}_1-\mathbf{x}_2)}\int dx\int dy\, xy e^{-(x^2+y^2)/2}\sin^{-1}\left[\frac{xyS^0(\tau)/2\gamma_{k_{\max}}}{(1+x^2Y/2\gamma_{k_{\max}})^{1/2}(1+y^2Y/2\gamma_{k_{\max}})^{1/2}}\right] , \tag{34}$$

with $S^0(\tau)=e^{2\gamma_{\mathbf{x}_{12}}t}\langle|\psi|^2\rangle(k,\tau=0)$ and $Y=\sum_{\mathbf{k}}S^0(\tau)$ and $\gamma_{\mathbf{x}_{12}}$ being the Fourier transform of γ_k.

IV. NUMERICAL INTEGRATION

In this section, we give details of our simulations and compare the results with the early-time theory outlined in Sec. III. Most of the simulations which we conducted were for quenches to zero temperature. The TDGL equation [Eq. (9)] was discretized using a standard finite-difference scheme.[18] The discretized equation was then integrated using both a Euler scheme and a fourth-order Adams-Bashford predictor and an Adams-Moulton corrector technique.[19] The simulations were performed on a CRAY XMP and a SUN 3/260 workstation. All the simulations were performed on an $N=128^2$ sized system with periodic boundary conditions. The dimensionless mesh size Δx and the dimensionless time step $\Delta\tau$ were chosen in such a way as to avoid possible spurious unphysical solutions resulting from the subharmonic bifurcation.[18] For the Euler scheme, we chose $\Delta x=1$ and $\Delta\tau=0.01$. Using the predictor-corrector method it was possible to use a larger time step of $\Delta\tau=0.1$. To check the stability of the predictor-corrector method, we com-

pared the solution it generated to a solution generated through a Euler scheme ($\Delta\tau=0.01$), finding that they differed at $\tau=30$ through a negligible relative error of less than 0.05%.

In the discretized TDGL equation, the integral term was evaluated by transforming into k space, multiplying by the discrete form of of $g(k)$, and then transforming back into real space. This proved to be particularly advantageous because of the availability and accuracy of fast-Fourier-transform routines.[19] We concentrated on quenched systems at zero temperature, since a detailed comparison between theory and simulation results is possible there. However, we did study a small number of systems at nonzero temperatures (i.e., $\epsilon \leq 0.1$) finding, however, no significant qualitative differences from the $T=0$ results.

The specific form of the long-range repulsive force chosen was for a uniaxial ferromagnetic system as described in Sec. II. The parameters characterizing the force were chosen in such a way as to obtain a linear dispersion relations γ_k as shown in Fig. 3. We studied systems with both stable and unstable long-wavelength modes. Table I summarizes the various parameters used. In all cases, except run E, the initial state was approximated by a random configuration with $|\psi(\tau=0)| \leq 0.01$. In run E, the initial state was a random configuration with $|\psi(\tau=0)| \leq 0.05$. The parameter values were chosen because they gave rise to patterns whose wavelengths were small compared to the system size. This is important, because finite-size effects can play a significant role if the stripe width is of the order of the system size. In such a case, it is difficult to observe the formation of modulated structures and the system configurations qualitatively resemble a Model-A system that is phase separating through domain growth. We tested a range of other parameter values, but they in no way altered the essential features of the model. Rather, changing the parameters allows one to tune the nonuniversal features such as the saturation value of the order parameter and the wavelength of the pattern. The predicted variation of these with the strength of the long-range repulsive force are shown in Fig. 5, for the case of a system with stable long-wavelength modes. Note that in the limit of $\beta=0$, the saturation value predicted is ± 1, and the wavelength of the pattern formed diverges so that the system is described by a phase-separated solution.

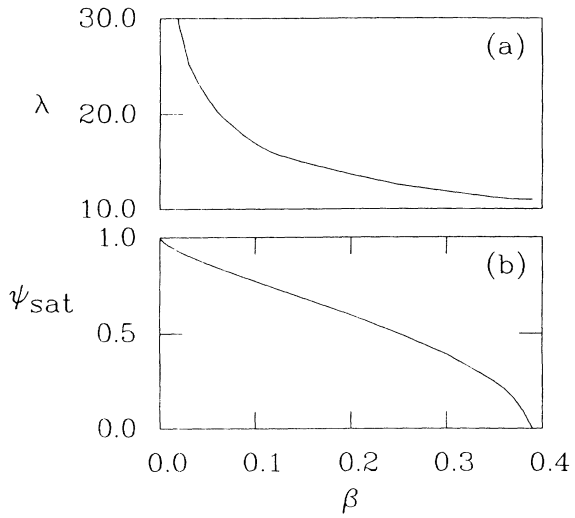

FIG. 5. (a) Variation of the predicted wavelength of the equilibrium ordered structure with the strength of the long-range force. Here $\lambda=2\pi/k_{\max}$, where $k_{\max}$ is the k vector for which γ_x is maximum. (b) Variation of the order parameter saturation value $\psi_{\text{sat}}=(\gamma k_{\max})^{1/2}$, with the strength of the long-range repulsive force. Here $L=50$.

A. Critical quench into the stripe phase

In this section, we present numerical results for critical quenches from the paramagnetic state into the stripe phase. System with both stable and unstable long-wavelength modes are considered.

Figure 6 shows the time evolution of the order parameter morphology for a system with *stable* long-wavelength modes (run E) at different times, as well as the order parameter contours of an arbitrary cut through the system. Small inhomogeneities in the initial conditions are amplified by the band of unstable modes, giving rise to stripe-like patterns broken up by dislocations. These dislocations arise because the free energy of the system is degenerate with respect to the direction of the unstable k vectors. Therefore, in a quenched system, each point in the system selects an independent direction, which leads to a convoluted and interconnected pattern. Initially, the dynamics is dominated by short-ranged attractive forces so that the early-time configurations [Figs. 6(a) and 6(b)] are similar to early-time Model-A configurations. Later

TABLE I. Parameters used in simulations. $k_{\max}$ is the maximally unstable wave number. N_q is number of independent quenches.

Run	β	L	h	$k_{\max}$	N_q	$\tau_{\max}$	n
A	0		0	0	5	200	$0.47_5\pm0.06$
B	0.1	0.5	0	0.006	5	200	$0.46_8\pm0.05$
C	0.1	5	0	0.270	5	200	0.16 ± 0.05
D	0.1	10	0	0.351	5	200	0.06 ± 0.06
E	0.1	50	0	0.368	5	200	$0.04_5\pm0.05$
	0.1	50	0	0.368	30	30	
F	0.1	50	1.0	0.368	10	30	

times [Figs. 6(c) and 6(d)] are dominated by the long-range repulsive force, which limits the growth of the domains, building up stripe-like patterns on short length scales. Notice that between $\tau=30$ and $\tau=300$, the stripe thickness has remained essentially unchanged. During this time interval the system tries to reduce its surface free energy by annealing away the curvature present in its interfaces and form stripes on long length scales. However, this process is highly ineffectual since the system is unable to overcome the large free-energy barriers associated with the dislocations. As a result, there is very little system evolution beyond $\tau=100$. Notice that the order parameter saturates at values well below ± 1. Configurations for systems with $L=1/\beta$ at low temperatures exhibit similar behavior.

The time evolution of the one-point distribution function $\rho(\psi)$ for run E is shown in Fig. 7(a). Initially, the distribution is a single peak centered about $\psi=0$. The peak then collapses and broadens. Finally, two symmetric peaks are built up about the saturation values of

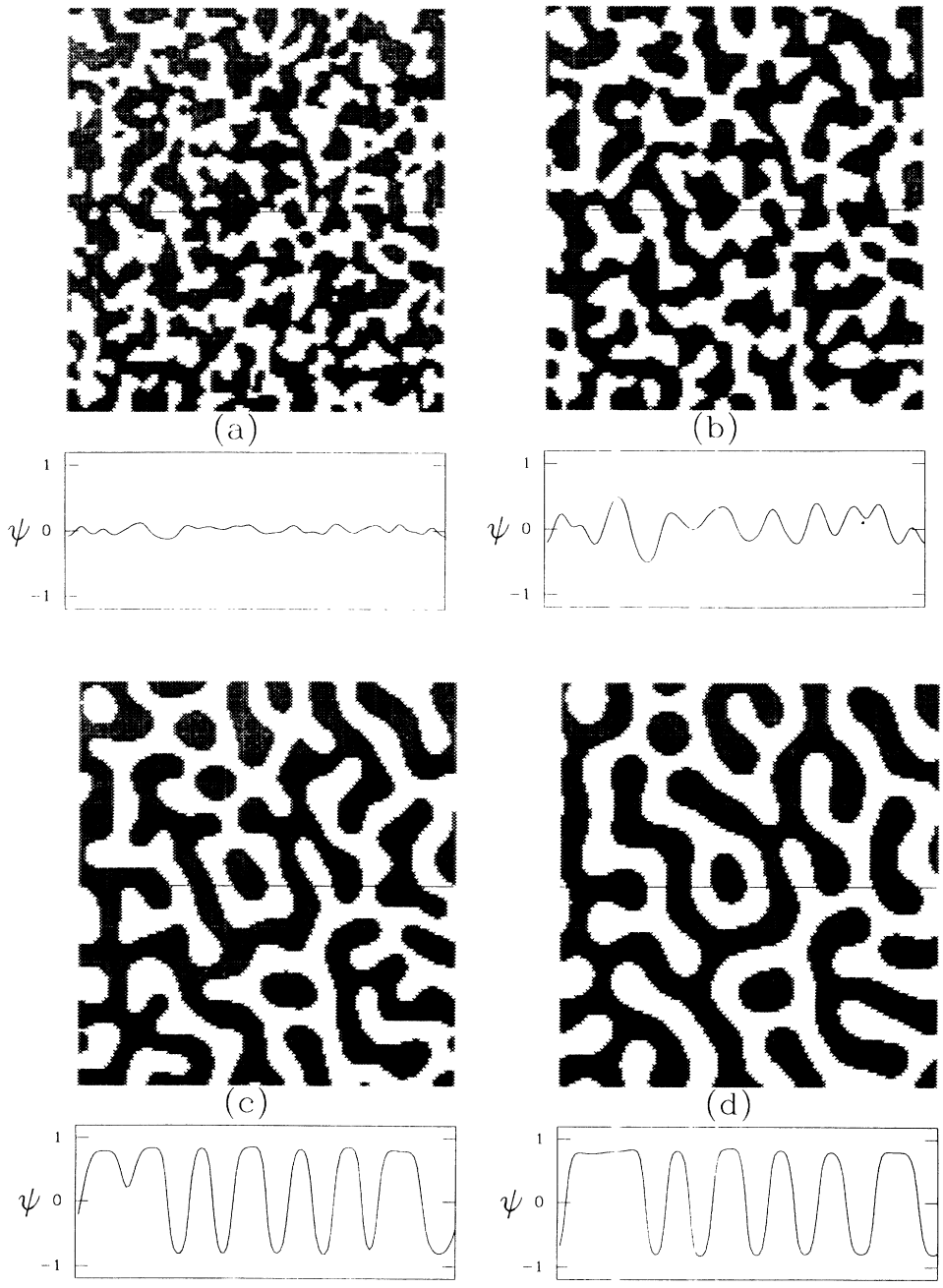

FIG. 6. Evolving domain structure of a $N=128^2$ system with stable long-wavelength modes (run E: $\beta=0.1$; $L=50$; $h=0$). Positive order-parameter values are marked. The solid line through the configurations mark the position of the order-parameter contour plots shown beneath the configurations. Times shown are (a) $\tau=2$, (b) $\tau=5$, (c) $\tau=30$, and (d) $\tau=300$.

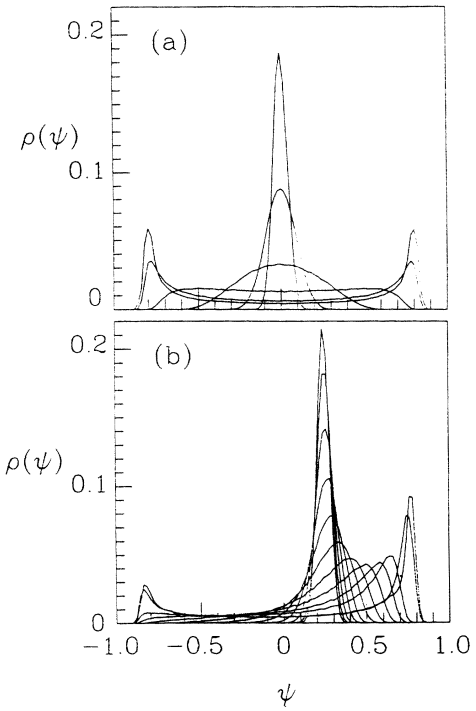

FIG. 7. Time evolution of the one-point distribution function $\rho(\psi)$ (run *E*). (a) For a quench into the stripe phase, i.e., $h=0$, in order of the decreasing peak about $\psi=0$ the times are $\tau=1,3,5,10,20,30$. The distribution function shown is the result of an average over 30 different runs with independent initial conditions. (b) For a quench into the bubble phase with $h=1$, in order of decreasing peak size about $\psi\approx 0.25$, for times $\psi=1,2,\ldots,10,15,30$. The distribution function is averaged over 10 different runs. Note the asymmetry in the final peak heights.

the order parameter.

To monitor possible domain growth, we studied the amount of interfaces present in the system. Figure 8 shows the inverse perimeter density (R_p) for a uniaxial ferromagnetic system. R_p, which is defined as the ratio

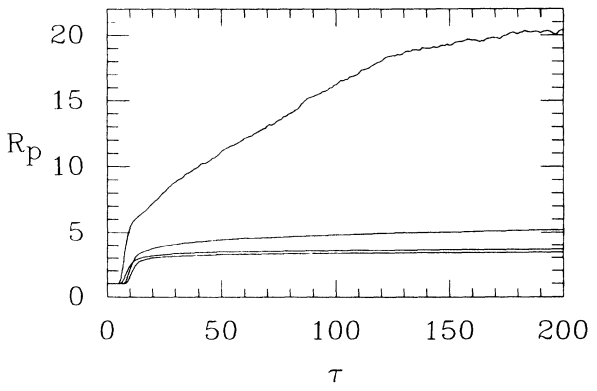

FIG. 8. R_p, the inverse perimeter density vs time. The lines at late times from top to bottom are for runs *B*, *C*, *D*, and *E*. Note that for systems with stable and marginally stable long-wavelength modes (runs *D* and *E*), the lines are almost coincident.

of the total number of sites to the number of interface sites, was calculated as follows: Any site with $\psi^2 \le 0.36\psi_{\rm sat}^2$ was counted as an interface site, otherwise, it was taken to be part of the bulk. The resulting data for these intermediate times were tentatively fit to a power law, i.e., $R_p = At^n + B$ with growth exponent n. The values of these effective growth exponents are given in Table I. Our results indicate that systems with unstable long-wavelength modes exhibit growth at intermediate times. This is because, for such systems, $k_{\rm eq}$ is smaller than $k_{\rm max}$ so that after stripe patterns of period $2\pi/k_{\rm max}$ are formed on small length scales, these stripes begin to thicken and coarsen until they are of thickness $2\pi/k_{\rm eq}$. At the same time the system tries to reduce the amount of surface free energy present by annealing way the curvature present in its interfaces. This process continues until the dominant length scale of the system corresponds to $2\pi/k_{\rm eq}$. Because the system is dominated by a single time-independent length scale, the growth process is not self-similar. The measured value of the effective growth exponent n changes continuously from $n=\frac{1}{2}$ for a system with no long-range force (i.e., $\beta=0$), to a possible $n=0$ value if the $k=0$ mode is stable.[20] For a system with stable long-wavelength modes there is significant growth only in the early states. At late times the system still tries to reduce the curvature present in its interfaces and produce stripes on long length scales. This process is, however, hampered by the presence of the dislocations, which at low temperatures eventually pin the interfaces.

We also obtained the two-dimensional structure factor, which is

$$S(\mathbf{k},\tau)=\left\langle \frac{1}{N}\left|\sum_{\mathbf{x}_i}\psi(\mathbf{x}_i,\tau)e^{i\mathbf{k}\cdot\mathbf{x}_i}\right|^2\right\rangle , \tag{35}$$

where $\mathbf{k}(2\pi/\sqrt{N})(m\hat{\mathbf{i}}+n\hat{\mathbf{j}})$, $m,n=1,2\ldots\sqrt{N}$, where $\sqrt{N}$ is the system length. The circularly averaged structure factor is

$$S(k,\tau)=\sum_{\mathbf{k}} S(\mathbf{k},\tau)\Big/\sum_{\mathbf{k}} 1 , \tag{36}$$

with $k=2\pi n/\sqrt{N}$, $n=0,1,2,\ldots\sqrt{N}$ and the sum $\sum_{\mathbf{k}}$ is over a circular shell defined by $n-\frac{1}{2}\le|\mathbf{k}|\sqrt{N}/2\pi \le n+\frac{1}{2}$. $S(k,\tau)$ is illustrated in Fig. 9. For a system with marginally stable long-wavelength modes (run D), as shown in Fig. 9(a), $S(k,\tau)$ is peaked about a nonzero k vector, $k_{\rm max}$. There is no significant wandering of the peak of the structure factor over the time regime considered indicating that crossover effects are negligible; here $k_{\rm max}\approx k_{\rm eq}$. There is, however, a crossing of the tails of the structure factor.

In contrast, crossover effects play an important role at late times if $k_{\rm eq}$ differs from $k_{\rm max}$. This effect is observed if the long-wavelength modes are unstable, becoming more and more marked as β approaches zero (runs *B* and *C*). This is illustrated by Fig. 9(b). At early times ($\tau\le 20$) the system builds up a stripe-like pattern of period $k_{\rm max}$, as is reflected in the initial peak of $S(k,\tau)$. After the contribution of this mode has saturated, the system dynamics is dominated by the $k_{\rm eq}$ which is smaller than

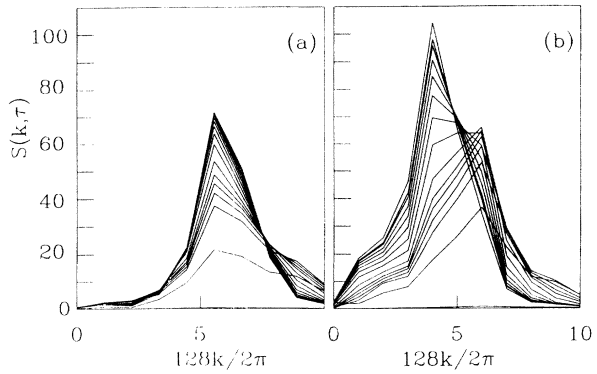

FIG. 9. Circularly-averaged structure factor $S(k,\tau)$ as obtained by numerical integration. (a) For run D in order of increasing peak size $S(k,\tau)$ at $\tau=5,10,15,20,25,30,40,60,\ldots,200$. (b) For run C in order of increasing peak size $\tau=5,10,15,20,25,30,40,60,\ldots,200$.

$k_{\max}$. This results in a thickening of the stripe-like pattern. The phenomena of mode saturation is a consequence of the nonlinearity. The rate of achieving this saturation is k dependent with smaller k modes taking a longer time to saturate. The consequent coarsening of the peak of $S(k,\tau)$ is a subtle effect, which is absent in KYG-like theory. For this system, crossover phenomena and the late-time interfacial dynamics are not yet fully explored and will be the subject of a future investigation.

We now compare our simulation results with those of the KYG solution. Figure 10 illustrates this by showing the time evolution of the order parameter contours taken from an arbitrary cut through a configuration generated by the simulation of a system with stable long-wavelength modes (run E) and the KYG equations. Both correspond to the same initial random configuration. There are no significant deviations between the simulation and KYG results for $\tau \lesssim 8$. Small deviations then occur, with the growth rate being consistently overestimated by the KYG solution. This is not surprising considering the approximations made: KYG technique takes the growth rate of all the modes to be that of the maximally unstable mode $k_{\max}$, which is incorrect and an overestimate for all other wave numbers. Note that the KYG solution predicts the saturation value of the order parameter at $\psi_{\text{sat}}=(\gamma_{k_{\max}})^{1/2}$, which agrees with the simulation results to within 5%. Note also that the KYG solution is a theory with a single length scale. It is therefore unable to correctly generate the finite interface width, any late-time coarsening phenomena, or the crossover from $k_{\max}$ to k_{eq}. Similar behavior was observed in the KYG solution for a system with unstable long-wavelength modes.

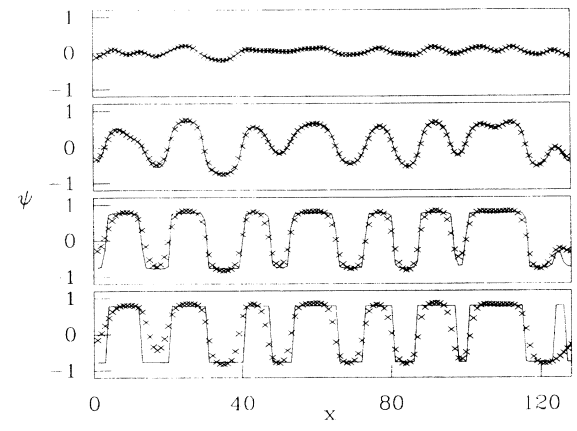

FIG. 10. Comparison of time evolution of order parameter as obtained through numerical simulation (marked by x, for run E) and the KYG solution (marked by a solid line). The contour plots shown represent arbitrary cuts through an evolving configuration. Shown from the top to the bottom panel are $\tau=3$, 7, 11, and 30.

To obtain a more quantitative comparison between the simulation and the KYG solution, the variance of $S(k,\tau)$ was studied (Fig. 11), i.e.,

$$\sigma^{\text{KYG}}(\tau)=\left[\sum_k [S^s(k,\tau)-S^{\text{KYG}}(k,\tau)]^2/\sum_k S^s(k,\tau)^2\right]^{1/2}, \tag{37}$$

where the sum is over all the k vectors, the index s denotes the simulation results, and the index KYG denotes the KYG solution. Figure 11 shows a similar comparison between the simulation and the linear theory. In a relatively short time the errors between the simulation and linear theory diverge exponentially, while the errors between the simulation and the KYG solution remain relatively constant. It seems, therefore, that the KYG solution provides an excellent description of the early-time dynamics of a system with a scalar nonconserved order parameter and with a long-range repulsive interaction.

B. Quenches into the bubble phase

We have also studied quenched from the uniform phase into the bubble phase, using the numerical methods discussed in Sec. III. In particular, ten independent quenches with $h=1.0$ were carried out (run F).

Figure 12 shows an example of such an evolving

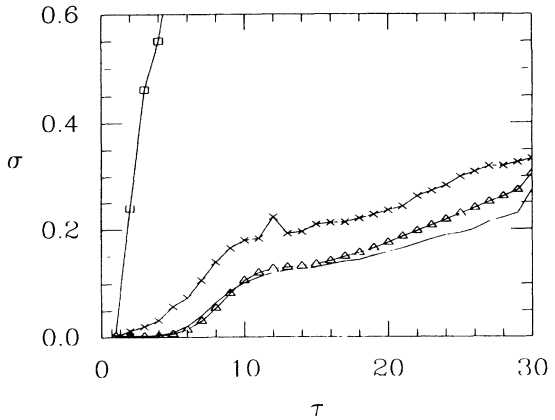

FIG. 11. Variance as defined in Eq. (33) vs time for (a) linear solution (squares) and KYG solution for run E (crosses), (b) KYG solution for run D (triangles), and (c) KYG solution for run C (solid line).

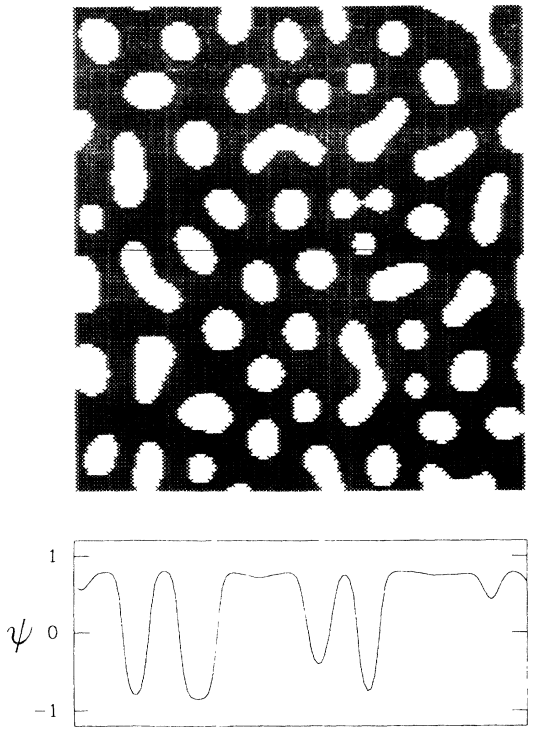

FIG. 12. Evolving domain structure of the long-range force system with nonzero external field $h=1.0$ (run f). Positive deviations from the average value of ψ are marked. The time is $\tau=30$. The solid line marks the position of the order-parameter contour plot shown below the configuration.

configuration at time $\tau=30$. Here, positive deviations from the system's average value of ψ are marked. In contrast to the percolating domain structure obtained from quenches into the stripe phase, the configuration consists of a sea of droplets. In many ways, this is visually similar to configurations obtained from off-critical quenches in Model-A of Model-B systems.[21]

The time-evolution of the one-point distribution function is shown in Fig. 7(b). Initially, the system is peaked about a single, nonzero value of ψ. This peak then begins to collapse as the phase separation proceeds, and later two asymmetric peaks are formed about the equilibrium values of ψ.

$S(k,\tau)$ was found to display very similar features to those of an $h=0$ quenched. Namely, $S(k,\tau)$ is peaked at about the same value of k and remains stationary over the time regime examined. The peak is, however, slightly broader and less sharp, narrowing slightly over time. This feature is most likely due to a distribution of droplet sizes. We have not studied the angular correlations of the structure factor, which are expected to display a hexagonal symmetry. Note that the general features of the circularly-averaged structure factor for the bubble phase are very similar to those of the stripe phase. The differences between the two phases are therefore better characterized by studying topological features of the two phases, e.g., cluster-size distributions.

We have also investigated the growth of the droplet over time, finding no significant differences from the $h=0$ case. Initially, there is extensive growth as the fluctuations in the initial state are amplified. The order parameter, however, soon saturates. There is very little growth in mean droplet size after about $\tau=30$, although the system still continues to evolve so as to form circular droplets and rearrange them as to attain a hexagonal symmetry.

V. CONCLUSIONS

We have studied the dynamics of pattern formation of a Model-A system with a long-range repulsive force. The presence of the long-range repulsive force leads to the formation of modulated structures. It changes the strictly local model, Model A, into a nonlocal model. By tuning the parameters describing the long-range repulsive force, one is able to alter stability of the long-wavelength modes of the system.

The dynamics of the formation of these modulated phases may be separated into an early- and a late-time regime. The early-time regime is dominated by the most unstable mode of the linear dispersion relation. This regime is well explained through an approximate solution based on a KYG expansion of the appropriate TDGL equation. This solution accounts for some of the nonlinearities present in the model. It yields a nonexponential growth rate of the order parameter, and a saturation value which seems to be correct within 5% of the value obtained in the numerical simulation. There are no significant differences between the KYG solution and simulation results at early times. At late times the system tries to evolve in such a way as to reduce its surface free energy. If the wave number of the equilibrium pattern differs significantly from the most unstable mode of the linear dispersion relation, a crossover takes place at late times which is not described by the KYG solution.

These results indicate the usefulness of the KYG approach in providing early-time solutions to a variety of time-dependent Ginzburg-Landau equations. In the future we will investigate systems with both long-range repulsive interactions and a strictly conserved order parameter.

ACKNOWLEDGMENTS

We would like to thank Martin Grant, Ken Elder, and Tim Rogers for many useful discussions. We also acknowledge with thanks the support for the Natural Sciences and Engineering Research Council of Canada. Some of the simulations presented in this paper were performed using the CRAY-XMP at the Ontario Center for Large Scale Computing.

[1]Reviews are given by J. D. Gunton, M. San Miguel, and P. S. Sahni, in *Phase Transitions and Critical Phenomena,* edited by C. Domb and J. L. Lebowitz (Academic, London, 1983), Vol. 8; K. Binder, Physica (Amsterdam) **140A**, 35 (1986), and references therein.

[2]S. M. Allen and J. W. Cahn, Acta Metall. **27**, 1085 (1979).

[3]I. M. Lifshitz and V. V. Slyozov, J. Phys. Chem. Solids **19**, 35 (1961).

[4]T. Garel and S. Doniach, Phys. Rev. B **26**, 325 (1982). Note that Eq. (1) of this reference leads to our Eq. (18).

[5]See, for example, D. Andelman, F. Brochard, and J. F. Joanny, J. Chem. Phys. **86**, 3673 (1987), and references therein.

[6]R. E. Rosensweig, M. Zahn, and R. Shumovich, J. Magn. Magn. Mater. **39**, 127 (1983).

[7]See, for example, P. de Gennes, *The Physics of Liquid Crystals* (Clarendon, Oxford, 1974).

[8]See, for example, W. L. McMillian, Phys. Rev. B **12**, 1187 (1975).

[9]J. R. Thomsen, W. Cowan, M. J. Zuckermann, and M. Grant, in *Proceedings of the XVIII Winter Meeting on Statistical Physics, Oaxatepo, Mexico, 1989,* edited by A. E. Gonzalez, C. Varea, and M. Medina-Noyola (World Scientific, Singapore, 1989); J. R. Thomsen, Z. Zhang, W. Cowan, M. Grant, J. A. Hertz, and M. J. Zuckermann (unpublished).

[10]K. Kawasaki, M. C. Yalabik, and J. D. Gunton, Phys. Rev. A **17**, 455 (1978).

[11]See, for example, A. P. Malozemoff and J. C. Slonczwski, *Magnetic Domain Walls in Bubble Materials* (Academic, New York, 1979).

[12]K. L. Babcock and R. M. Westervelt, Phys. Rev. Lett. **63**, 175 (1989); Phys. Rev. A **40**, 2022 (1989).

[13]C. Kooy and U. Enz, Phillips Res. Rep. **15**, 729 (1960); W. F. Druyvesteyn and J. W. Dorleijn, *ibid.* **26**, 11 (1971); J. A. Cape and G. W. Lehman, J. Appl. Phys. **42**, 5732 (1971); J. A. Cape, *ibid.* **43**, 3551 (1972).

[14]M. Suzuki, Prog. Theor. Phys. **56**, 477 (1977).

[15]See, K. Elder, Ph.D. thesis, University of Toronto, 1989 for an analogous calculation as applied to model-B systems.

[16]M. Abramowitz and I. Stegun, *Handbook of Mathematical Functions* (Dover, New York, 1972), Chap. 15, Eq. (15.1.1).

[17]We note that our approximations are possible here. For example, if $\gamma_k \approx 0$, then $F(\frac{1}{2},1;\alpha_k,z) \approx F(\frac{1}{2},1;\frac{3}{2},z)$ which has a simple analytic form. Such an approximation would clearly underestimate the growth of the nonzero k modes.

[18]A more detailed description of the discretization scheme is given in T. M. Rogers, K. R. Elder, and R. C. Desai, Phys. Rev. B **37**, 9638 (1983).

[19]W. H. Press, B. P. Flannery, S. A. Teukolsky, and W. T. Vetterling, *Numerical Recipes* (Cambridge University, Cambridge, MA, 1986).

[20]Due to the small number of runs, the values of the effective growth exponents are not very accurate. Furthermore, in two dimensions, it is possible that the long-range repulsive force gives logarithmic time corrections to the mobility, which, over the short-time regime studied, appear as reduced growth exponents.

[21]K. Elder and R. C. Desai, Phys. Rev. B **40**, 243 (1989); T. Rogers and R. C. Desai, *ibid.* **39**, 11 956 (1989).

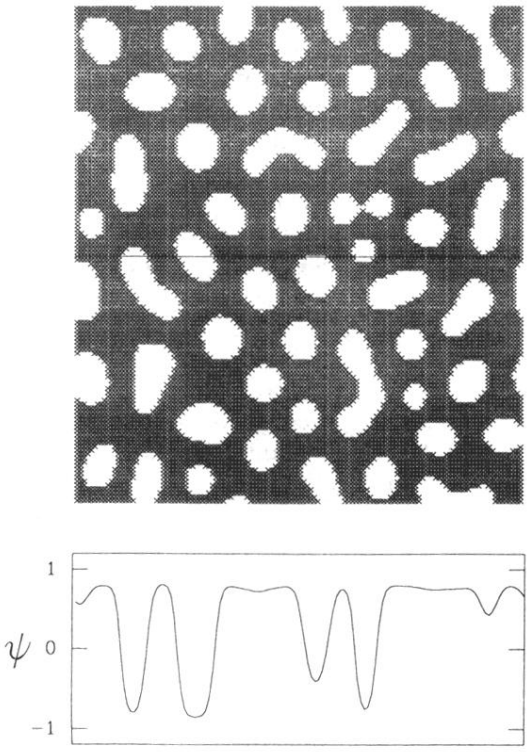

FIG. 12. Evolving domain structure of the long-range force system with nonzero external field $h = 1.0$ (run f). Positive deviations from the average value of ψ are marked. The time is $\tau = 30$. The solid line marks the position of the order-parameter contour plot shown below the configuration.

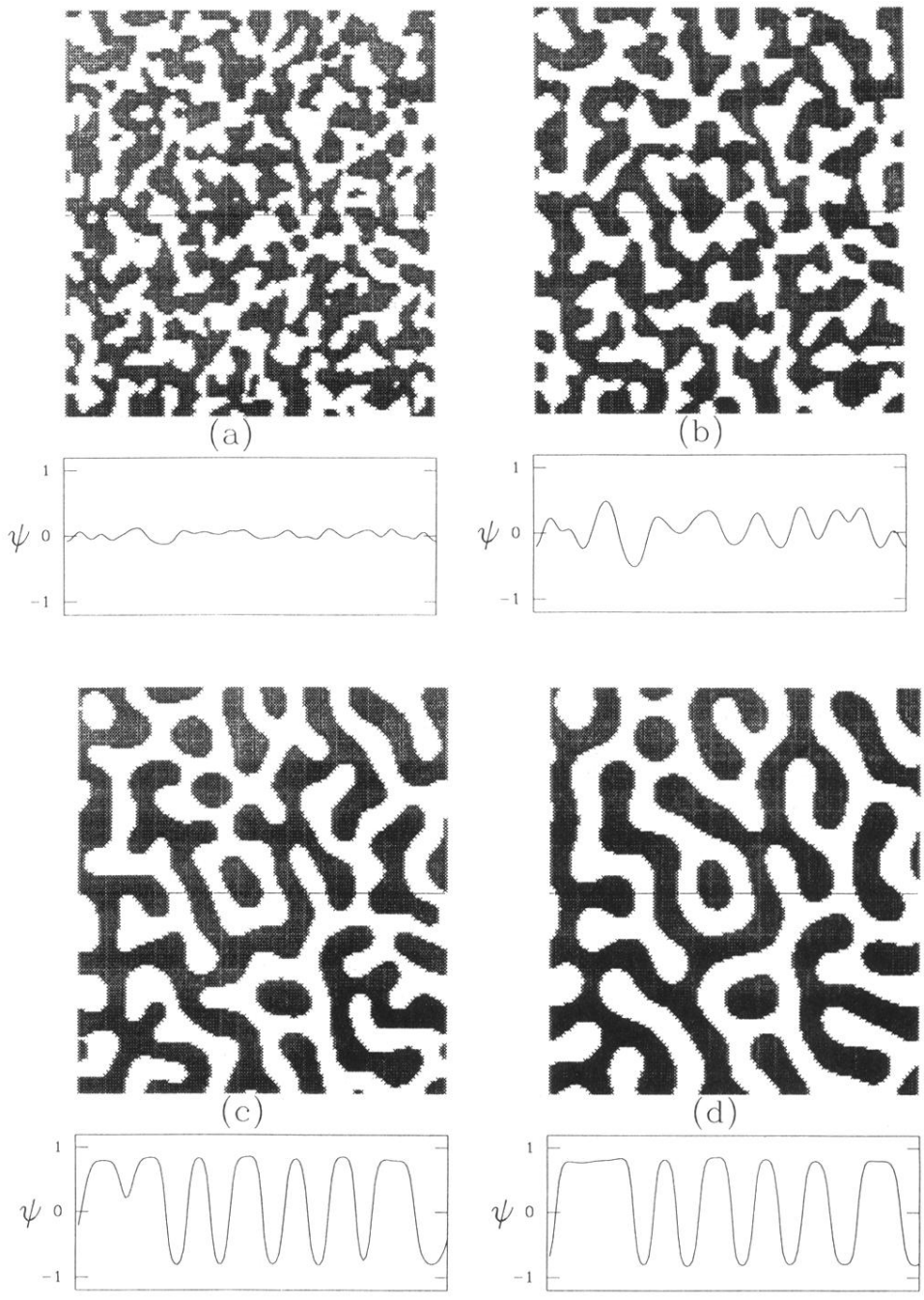

FIG. 6. Evolving domain structure of a $N=128^2$ system with stable long-wavelength modes (run E: $\beta=0.1$; $L=50$; $h=0$). Positive order-parameter values are marked. The solid line through the configurations mark the position of the order-parameter contour plots shown beneath the configurations. Times shown are (a) $\tau=2$, (b) $\tau=5$, (c) $\tau=30$, and (d) $\tau=300$.